

Tectonics and Sulphide Mineralization in the Boundiali Birimian Formations by Means of Geophysical Data

Simon Pierre Djroh^{1*} , Loukou Nicolas Kouamé¹, Serge Pacôme Déguine Gnoleba², Yapo Abolé Serge Innocent Oboue³, Boko Célestin Sombo¹

¹Applied Geophysics Research Team Laboratory, Mineral and Energy Resources (LGRME), Faculty of Earth Science and Mineral Resources, Félix Houphouët Boigny University, Abidjan, Côte d'Ivoire

²Ministry of Mines and Geology, Yamoussoukro, Côte d'Ivoire

³School of Earth Sciences, Zhejiang University, Hangzhou, China

Email: *djrohsp@gmail.com

How to cite this paper: Djroh, S. P., Kouamé, L. N., Gnoleba, S. P. D., Oboue, Y. A. S. I., & Sombo, B. C. (2022). Tectonics and Sulphide Mineralization in the Boundiali Birimian Formations by Means of Geophysical Data. *Journal of Geoscience and Environment Protection*, 10, 32-45.

<https://doi.org/10.4236/gep.2022.1010003>

Received: July 28, 2022

Accepted: October 15, 2022

Published: October 18, 2022

Copyright © 2022 by author(s) and Scientific Research Publishing Inc.

This work is licensed under the Creative Commons Attribution International

License (CC BY 4.0).

<http://creativecommons.org/licenses/by/4.0/>



Open Access

Abstract

This study focused on the interpretation of geophysical data collected from the Sissédougou prospect which is located at the southern end of the Korhogo-M'Benguebirimian trench. The geophysical surveys were carried out on two grids with two magnetometers and an induced polarisation unit composed of a transmitter and a receiver. The magnetic data allowed on one side the mapping of basic, intrusive and volcanic formations, weakly magnetic rocks produced by meta-sediments to be showed, and on the other hand to identify the continuity of the shear corridor observed southward and northward of the prospect. Induced polarisation data revealed the signature of sulphide and disseminated mineralization. The synthesis of the obtained results showed that deep NE-SW, NNE-SSW and N-S oriented fractures promoted the late rise of sulphide fluids. The setting of sulphide and gold mineralization in the southern part of the Boundiali trench is therefore controlled by ductile and brittle shearing.

Keywords

Geophysics, Shear Zone, Gold Sulphite, Birimian, Côte d'Ivoire

1. Introduction

In Côte d'Ivoire, sulphide gold mineralization is generally associated with greenstone belts which generally form an NNE-SSW oriented volcano-sedimentary furrow (Milesi et al., 1989; Allou, 2014; Coulibaly, 2018). The Korhogo-M'Bengue

trench is a typical example because it contains, in its northern part, the Tongon gold deposit which is controlled by hydrothermal fluids (Fofana et al., 2021).

Similarly, mining exploration work carried out on the Sissedougou prospect, which is located south of the Boundiali-Tengrela trench, has also revealed occurrences of gold mineralization (Doumbia, 2013).

Thus, this work aims to contribute to the improvement of knowledge on the setting up mode of gold sulphides mineralization in the southern part of this trench based on geophysical data.

2. Geographical and Geological Context

Both studied sites are located southward of Boundiali, northern Côte d'Ivoire (Figure 1). They are situated at the southern end of the Boundiali-Tengrela and Korhogo-M'Benguebirimian furrows, which extend into Mali and Burkina Faso through the Bagoue basin (Yacé, 2002). According to Couture (1968) & Doumbia (2013), the geology of this area is composed of meta-sediments, orthogneiss and micro-diorite, porphyroid granite and calc-alkaline granite, to which quartzites and volcano-sediments are associated. The meta-sediments, which occupy most of the prospect, are composed of undifferentiated schists, meta-conglomerates and meta-arkoses; all affected by greenschist facies metamorphism (Figure 2). However, orthogneisses occur in the eastern part, while

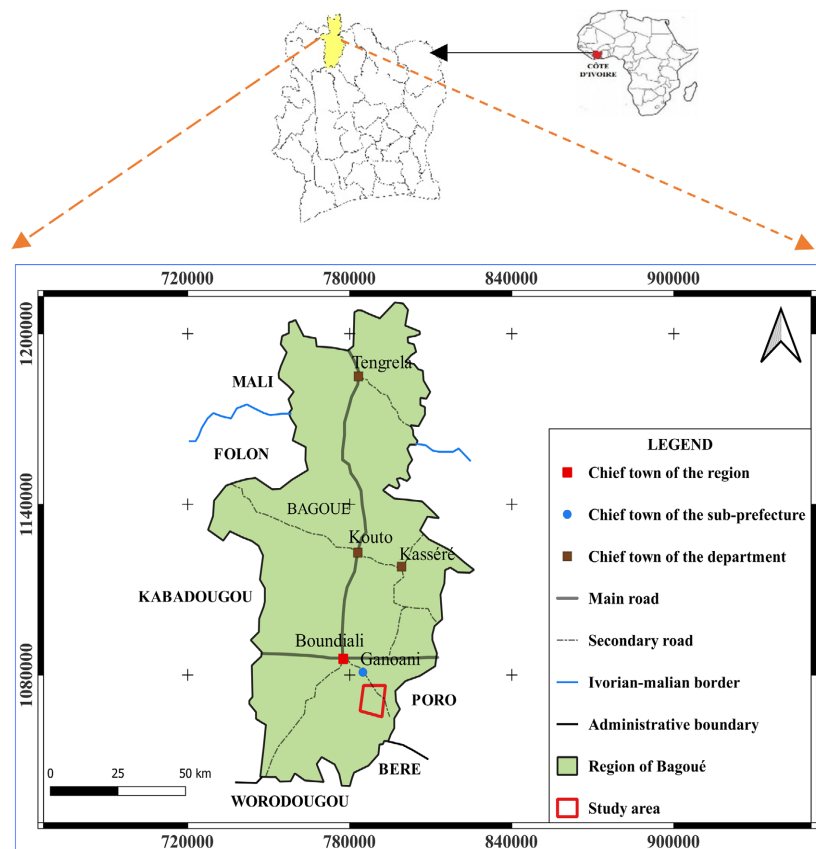


Figure 1. Location of the study area.

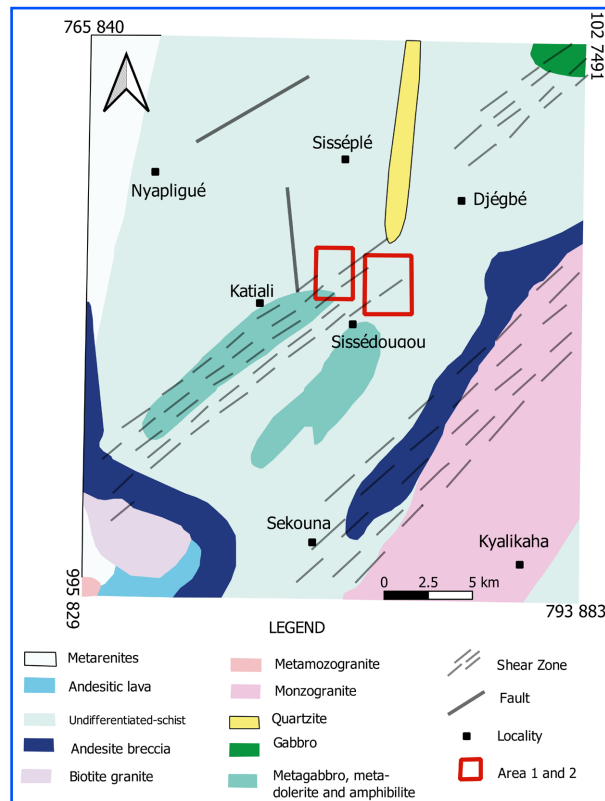


Figure 2. Geological map of the study area (Tagini, 1971).

quartzites and meta-microdiorites occur in the north and west as well as south area, respectively. Porphyroid granites are also observed in the southern part of the prospect and extend to the west.

3. Methodology

3.1. Magnetometry

Magnetic data were acquired with a 100×25 meters survey grid. Two G858 Sx Cesium magnetometers from Geometric were used, one in walk mode and the other one at the base station, the values of which were used for diurnal corrections. Afterwards, Fast Fourier Transform (*FFT*) filters were applied to the field values to produce different magnetic anomaly maps:

Reduction at the equator (REQ) was applied to correct the asymmetry of the signals created at low latitudes in order to facilitate the interpretation of the magnetic sources.

According to Verduzco et al., (2004), this correction is made with the following equation:

$$REQ(\theta) = \frac{[\sin(I) - i \cdot \cos(I) \cdot \cos(D - \theta)]^2 \cdot [-\cos^2(D - \theta)]}{[\sin^2(I_a) + \cos^2(I_a) \cdot \cos^2(D - \theta)] \cdot [\sin^2(I) + \cos^2(I) \cdot \cos^2(D + \theta)]} \quad (1)$$

where D : is the declination of the geomagnetic field, I : represents the inclination of the geomagnetic field, I_a : is the corrected inclination, θ : is the latitude of the

measurement point, $F^2 = -1$.

Upward continuation (Upwc) is a powerful filter that enhances the magnetic signatures of deep sources by bringing the data measured at a height h_0 from the ground surface to a height h_n higher than the observation plane. According to Thurston & Smith (1997), the simplified mathematical expression is given by the Equation (2):

$$L(r) = e^{-hr} \quad (2)$$

where h is the sensor-to-ground surface distance and r is the magnetic wave number per unit of measurement.

Tilt Derivation (TDR) is used to emphasise and strengthen long frequency, short wavelength anomaly signals from shallow magnetic sources. It is very useful in the identification of tectonic structures. Miller & Singh (1994) described the derivative of Tilt which was later developed by Salem et al. (2008) as equation (3). It is a function of the ratio between the vertical (first) and horizontal (x and y directions) derivatives:

$$TDR = \arctan\left(\frac{VDR}{THDR}\right) \quad (3)$$

with VDR (vertical first derivative):

$$VDR = \frac{\partial F}{\partial z} \quad (4)$$

and THDR (Total Horizontal Derivative):

$$THDR = \sqrt{\left(\frac{dF}{dx}\right)^2 + \left(\frac{dF}{dy}\right)^2} \quad (5)$$

where F is the value of the total magnetic field.

3.2. Induced Polarisation (IP)

For the surveys (IP), a transmitter (5000 watts) from Canadian GDD instrumentation and an IP receiver (*Elrec Pro*) from Iris instruments were used in time domain with rectangle gradient device. The injection cycle was 8 seconds and is provided by a bipolar wave with polarity inversion. In this mode, the IP effect is obtained, by the ratio of the maximum primary voltage (V_p) during injection and the secondary voltage ($V_s(t)$) at current cut-off. The apparent resistivity (ρ_a) is obtained with the following Equation (6):

$$\rho_a = \frac{V_p}{I} \times 2\pi K \quad (6)$$

where I is the current value, K : the geometrical characteristics of each measuring station.

The secondary potential ($V_s(t)$) is integrated under ten (10) time windows, M_i to M_{10} , and are defined by Equation (7) (Figure 3):

$$M_i = \frac{1}{V_p} \int_{t_1}^{t_2} v_s(t) dt \rightarrow M_i = \frac{V_s}{V_p} \quad (7)$$

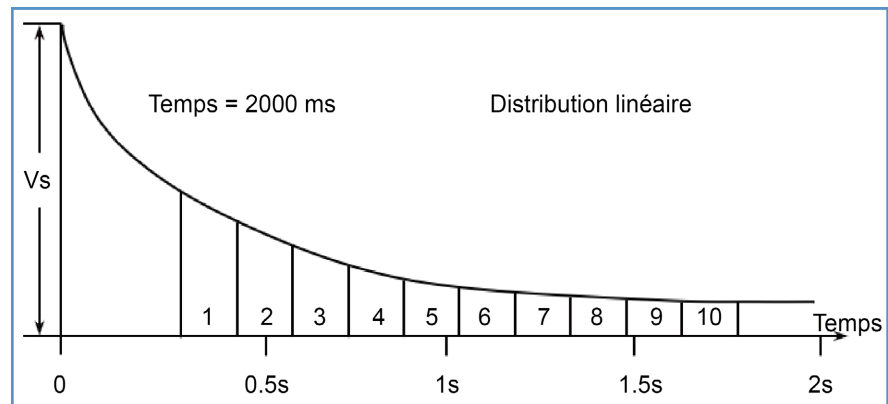


Figure 3. Integration of the secondary voltage for a linear distribution (Sagax, 1989).

with M_i partial chargeability, t_1 and t_2 the integration times of a window.

The corresponding chargeability value is the arithmetic mean of M_i and is determined according to Equation (8):

$$M = \frac{\sum_{i=1}^{10} 160ms * M_i}{1600ms} \quad (8)$$

4. Results and Discussion

4.1. Magnetometry

The magnetic field of the prospect has an amplitude of 445 (32290-31845) nanotesla (nT). This is a relatively small intensity, reflecting a quiet magnetic domain. Nevertheless, the application of the filters allowed us to discriminate three magnetic facies and important tectonic structures on the two sites (**Figure 4**). As far as the magnetic facies are concerned, we have identified three (3). The first highlights a series of fairly strong magnetism located north of the sites (1 & 2). It has an amplitude of 140 nT (32150-32290) and is mainly oriented NE-SW. This unit covers the northern half of both sites and corresponds to the signatures of rocks poor in ferromagnesian minerals such as undifferentiated shales represented on the regional geological map of the Sissedougou prospect. The second unit is characterised by a medium magnetic intensity with an amplitude of 60 nT (32090-32150).

It occupies the central parts of the sites and follows the E-W direction. This unit, which is more extensive at site 2 than at site 1, could be associated with the meta-arenites, meta-conglomerates and meta-arkoses defining the meta-sediments on the geological map. These magnetic facies would mark the transition between the two other units (strong and weak magnetic facies), reflecting a magnetic halo zone (**Figure 4**).

The third and last magnetic unit is associated with low magnetic field values with an amplitude of 245 nT (31845 to 32090). It occupies the southern part of the prospect and is oriented NE-SW (**Figure 4**). It corresponds to the deep magnetic signatures of rocks rich in ferromagnesian minerals such as meta-gabbros, meta-dolerites and meta-diorites or andesitic lavas shown in

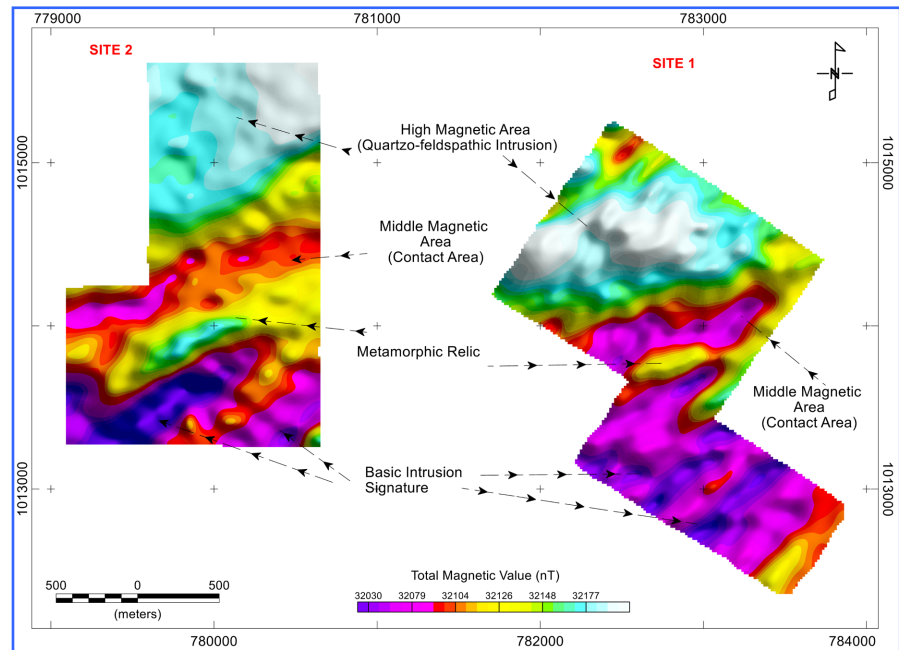


Figure 4. Reduced magnetic field map to equator.

the southern part of the geological map (see **Figure 2**). On the map of the reduced field at the equator (*REQ*), this unit is divided into several juxtaposed corridors between which the first two magnetic units are interspersed. This organisation makes the basic units rather narrow, elongated shapes, the dykes (**Figure 4**). The Upward Continuation map easily shows that the quartzo-feldspathic ensemble disappears in depth in favour of a more spread-out basic unit (**Figure 5**). This indicates that these acidic units intercalated between the basic rocks do not develop at depth, but are the magnetic response of quartzo-feldspathic relics from the contact metamorphism associated with basic intrusion to the south of the prospect (**Figure 4**). The magnetic response of these relics is identical to the signature of facies 2 described above. They are the site of element remobilisation that favours sulphide mineralization. The disappearance in depth of this unit makes it possible to establish a relative chronology for the emplacement of the different lithological units with the gabbro-diorites and dolerite-andesites which would mark the final phase of the eburnean orogeny (Tagini, 1971).

From a structural point of view, the examination of the magnetic signatures reveals the presence of two phases of displacement (**Figure 6**). The first phase is characterised by a North-South movement. This is marked by faults that affect all the magnetic facies, causing a shift in the structures from north to south. At site 1, this phase is expressed by faults that are only oriented NW-SE. At site 2, it is marked by faults that are mostly oriented NW-SE but, some are NNW-SSE and N-S.

A second, more recent tectonic phase is marked by NE-SW decays. It affects the different magnetic facies as well as the faults described above.

This phenomenon causes the banding of different structures through movements,

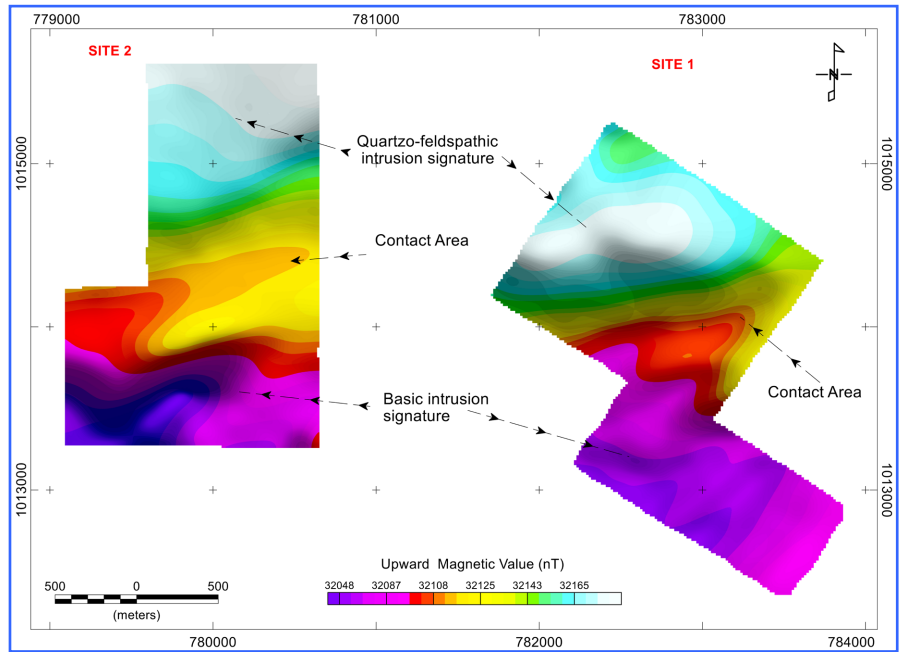


Figure 5. Upwards Continuation field map.

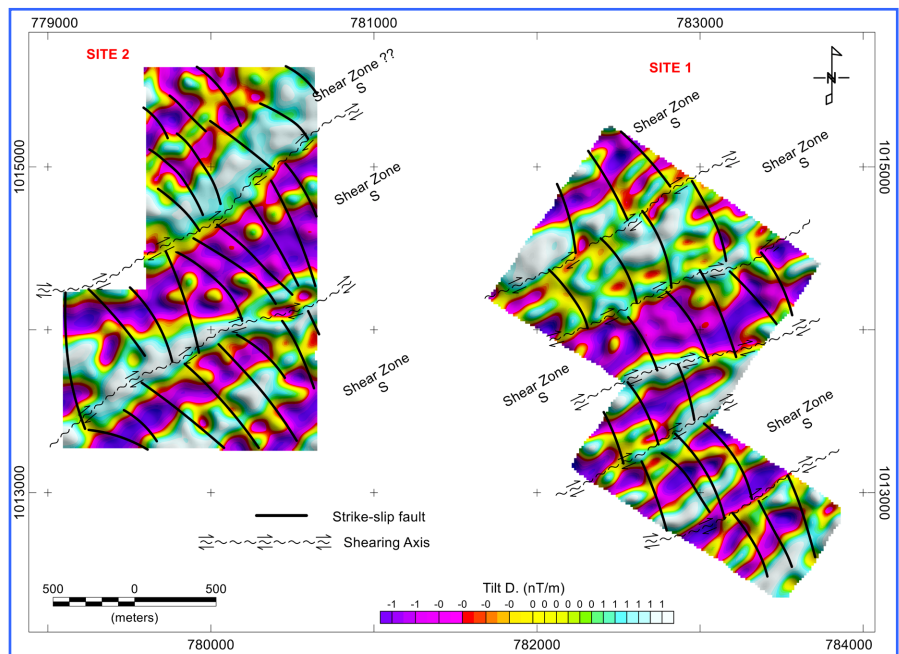


Figure 6. Tilt Derivation map.

in the NE and SW directions, which are marked by conjugated axes of dislocation.

The bands, defined by two axes, show a south-eastward slip on their northern edge, while the southern edge shifts to the north-east; characterising a sinister shear. These shear bands affect the whole site 1 and the central zone of site 2. This second tectonic episode thus marks the existence of shear bands which were mentioned by the Geological and Mining Research Office (BRGM) during re-

connaissance work carried out between 1988 and 1991 (see **Figure 2**). Site 1 and the central part of Site 2 are marked by a NE-SW ($N40^\circ$) shear.

4.2. Induced Polarization

The electrical data produced apparent polarization (chargeability) and resistivity maps. The first physical parameter reflects the response of the sulphide mineralization and the second characterises the electrical diffusion of the host rock.

The resistivity map shows important conductive and resistive structures. They are narrow and mainly oriented NE-SW at site 1 and N-S at site 2 (**Figure 7**). There is also a resistive axis occupying the centre of site 2 and oriented NE-SW. The apparent resistivities of the prospect range mainly from 178 to 13483 $\Omega\cdot m$.

Figure 8 shows some nice polarisable anomalies with chargeability values ranging from 8 to 21.1 mV/V. They follow the same directions, namely NE-SW and N-S, as the resistive structures identified at both sites. Most of the polarising axis in the prospect is associated with high electrical resistivity structures; with the exception of a polarising and conductive corridor located to the south of Site 1. From a geological point of view, this association reflects the electrical signature of sulphides disseminated in a silicified matrix such as quartz veins and veinlets.

These polarisable structures have also been obtained at the Goumere gold prospects, located in the Dimbokro-Fetekro trench (Aka, 2018), and in the greenstone belts of eastern Botswana (Sono et al., 2020). However, it should be noted that chargeability is higher for graphitic (Heritiana et al., 2019) or copper-nickel (Djroh, 2014) mineralization with values above 30 mV/V.

Four (4) main polarisable axis are highlighted at site 1 (**Figure 8**). They are

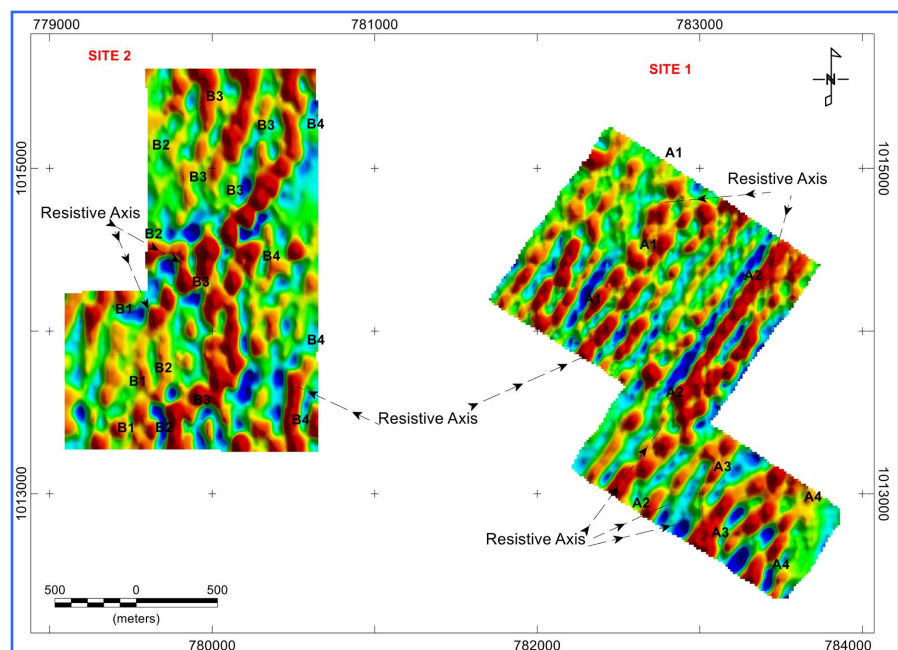


Figure 7. Apparent resistivity map.

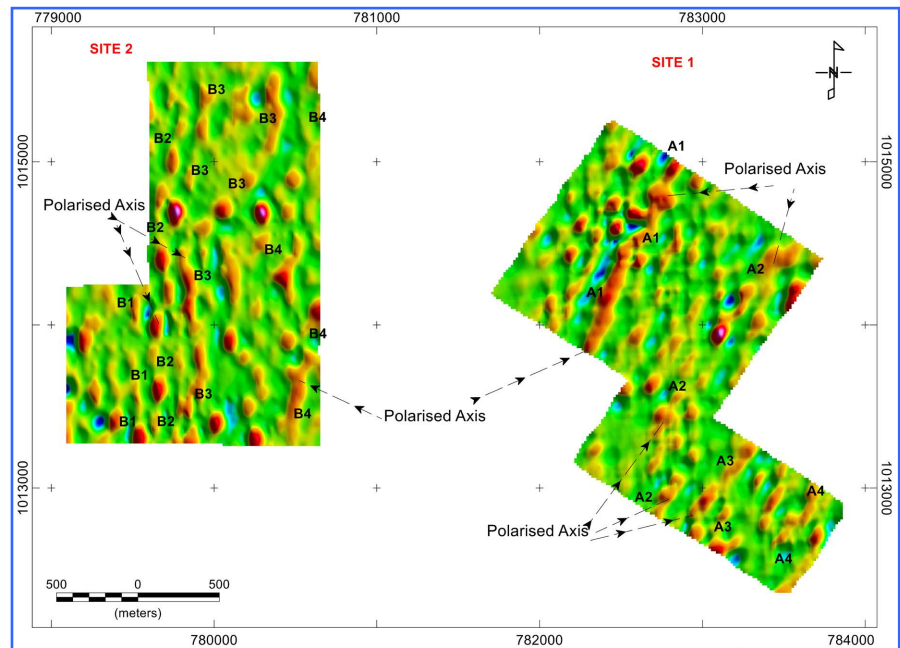


Figure 8. Apparent chargeability map.

labelled **A₁** to **A₄**, and are elongated in a NE-SW direction. The **A₁** axis, which is more expressive than the others, is located in the western part of site 1. It presents enough distortions, but remains interrupted and develops in the N30° direction. It constitutes the main polarising corridor of Site 1. The **A₂** axis, located in the centre of Site 1, is discontinuous and shows more distortion than the **A₁** axis.

It bifurcates in its northern part into two branches of NE-SW direction. Its intensity decreases from North to South where it reaches 8mV/V. The **A₃** and **A₄** axis are located to the south of Site 1 and have the same geometrical characteristics as the previous ones, but with a moderate intensity. Overall, axis **A₁** to **A₃** are associated with silicified rocks, while axis **A₄** is linked to a conductive corridor, which is thought to be the site of accumulation of hydrothermal alteration products.

Site 2 also has four (4) major polarising axis noted **B₁** to **B₄** (Figure 8). They are all oriented N-S with the exception of axis **B₃**, which develops a second branch to the north, oriented towards the North-East.

Axis **B₁** and **B₂**, which occupy the western edge of the study area, are discontinuous and form boudins with moderate polarisation intensity. Axis **B₃** occupies the central part of Site 2, and is fairly continuous compared to the other two and has a relatively higher polarisation intensity. It shows some distortions due to the effects of secondary faults. Polarising axis **B₄** is located in the south-east and develops towards the north. It is quite discontinuous and has a weak polarisation to the north and a medium polarisation to the south (Figure 8).

Axis **B₁**, **B₂** and **B₄** are associated with medium resistivity rocks with values below 3294 Ω·m. They are therefore linked to lithological contacts which are

characterised by intermediate resistivity values. Axis **B₄** is superimposed on the signature of a high resistivity rock with values above 5600 $\Omega \cdot m$ (**Figure 8**), a major characteristic of disseminated sulphide-bound gold mineralization. Indeed, an association of geological elements formed by the dissemination of gold, pyrite and chalcopyrite in a quartz matrix produces a geophysical signature of high resistivity and chargeability (Aka et al., 2017; Moreira et al., 2016).

4.3. Synthetic Analysis

The magnetic data show a better spatial distribution of the geological formations in this prospect. They locate at depth the basic rocks to the south and the silicified rocks to the north (see **Figure 5**). On the overlying levels to these two main units, magnetic transitional facies is interspersed in places, marked by meta-sediments. This facies reflects the interaction between the basic intrusion and the schistose host rock, which causes the formation of quartzo-feldspathic relics that are intercalated between basic corridors, thus creating zones of remobilisation elements (see **Figure 6**).

The superposition of the polarisable and resistive axis on these geological units contributes to elucidate the context of the setting of the identified gold mineralization (**Figure 9**). At Site 1, the polarisable and resistive axis intersect the geological units obliquely and make an angle of about 40° with the main shear direction. This orientation is reminiscent, according to Riedel model, of the formation of deep openings that would favour the accumulation of silicified fluid. Thus, the loadable axis associated with the resistive corridors would have been set up by the stretching created by the stretching shaped by the movements due to the effects of the shearing that affected Site 1. In fact, the dextral displacements cause deep cracks in the flattening direction (plane oblique to the direction of the main shear) that are substantially oriented N40°. These would be filled by residual post-tectonic crystallisation fluids; fluids resulting from the remobilization of elements and which are known to be rich in silica and poly-metallic sulphides. The flattening plane being oblique to the main shear direction, this explains the proximity in orientation of the electrical and magnetic signatures of Site 1. It is therefore important to note that the polarisable anomalies are not associated with the magnetic units (strong to weak), but rather with the silicified corridors which are characterized by medium to strong resistivities (**Figure 9**). Thus, the secondary polarisable axis **A₂** to **A₄**, of high resistivity, would be associated with the quartz vein while the main axis **A₁**, of medium resistivity, would be associated with the silicified structures.

For the second site, the direction of the electrical signatures contrasts more clearly with the geological formations (**Figure 9**). It's oriented N-S for the polarizable axis and NE-SW for the magnetic units. It is therefore highly unlikely that the genesis of the gold mineralization at Site 2 was controlled by the lithology. In a similar way to the first site, the polarising and resistive axis characterise

the sulphide and silicified polymetallic concentrations. The latter are also thought to be emplaced by the deep breaks, in the N-S oriented flattening plane created by the sinistral NE-SW shear. Indeed, the NE-SW shearing movement causes open fractures by stretching in the plane oblique to the main shearing direction. These cracks would be filled by post-tectonic crystallization fluids that remobilise silica and polymetallic sulphides including gold. Thus, the secondary polarisable axis **B₁**, **B₂** and **B₄**, of high resistivity, would also be associated with the quartz veins while the main axis **B₃**, of medium resistivity, would be linked to the quartz veins.

In view of the geophysical signatures, the sulphite mineralization at sites 1 and 2 would therefore be linked to a structural manifestation favoured by dextral transcurrent faults. The case of Sissedougou is similar to that of the Agbahou gold deposit where the mineralization is controlled by a major NE-SW trending shear zone that straddles the mafic volcanic and volcano-sediment contact (Houssou, 2013). According to this author, the shear is transcurrent, reverse sinistral and the main faults are oriented NE and NW. The ductile and cracking character of the shear would have favoured the upwelling of hydrothermal fluids and the formation of the gold-bearing quartz veins of Agbahou.

The major faults in the study area follow the same directions as those obtained in the Dabakalaregion by Gnanzou (2014). They strike N-S to NNE-SSW and NW-SE. Their effects contributed to the emplacement of the Bobosso gold mineralisation in the volcano-sediment series.

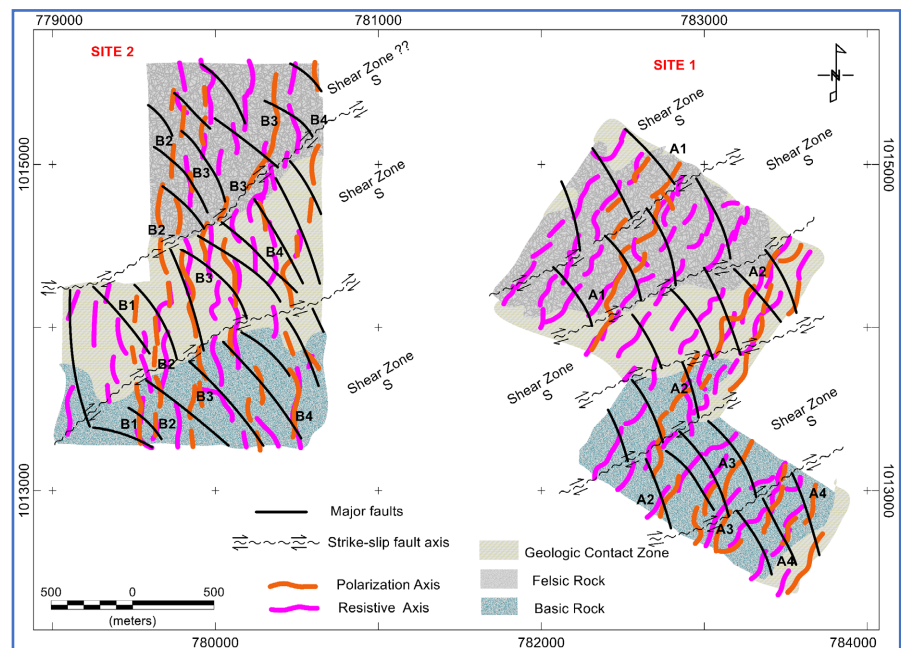


Figure 9. Synthesis map: shows the different magnetic domains, the major NW-SE faults and the NE-SW dextral strike-slip fault that created a sinistral shear corridor. The displacements caused deep openings in the basement where silicified gold sulphides were deposited by hydrothermalism.

Furthermore, geochemical studies carried out in the Korhogo-M'Bengué trench have shown, for the Tongon gold deposit, indications that characterise hydrothermalism. In this trench, where study's area is located, the formation of quartzo-feldspathic veins associated with sulphides, carbonates and sericite marks hydrothermalism (Fofana et al., 2021). In the Toumodi-Fétékro trench, these hydrothermal markers have also been highlighted in Agbahou (Houssou, 2013), Bonikro (Ouattara, 2015), Dougbafla (Ouattara, 2018) and Bobosso prospect in Dabakala region (Gnanzou, 2014).

The study of Angovia deposit also revealed brittle deformations of various directions, along which dextral or sinistral decays are often observed, and mineralised quartz veins at the level of the spandrels. The mineralization hosted in the andesito-basaltic volcanics is therefore favoured by hydrothermalism linked to NW-SE dextral and NE-SW sinistral conjugate faults (Koffi et al., 2013). Therefore, the gold mineralization of the Sissedougou prospect would probably be associated with hydrothermalism as it presents a similar geological and structural context in a trench dominated by hydrothermal mineralisation.

5. Conclusion

The present study has greatly contributed to the structural knowledge of the Sissedougou prospect. Magnetometry reveals that its geology is dominated by a basic intrusion, located in the South and North and composed of meta-gabbro and/or meta-dolerite, and a quartzo-feldspathic complex in the Centre which is marked by undifferentiated schists. Between these two units, reworked rocks characterised by meta-arkoses and/or grauwacke are interspersed. The tectonics is mainly marked by dextral (NE-SW) striking faults which define a major NE-SW (N40°) oriented shear corridor. The stretching associated with the deformations caused deep openings in the plane oblique to the main shear direction, which concentrated the polymetallic fluids in polarisable corridors that are oriented NNE-SSW (Site 1) and N-S (Site 2). Tectonic would thus have favoured the upwelling of hydrothermal fluids in the Sissedougou Birimian formations. It would therefore be important, for future work, to combine 2D reverse sections (geophysical) in order to identify not only the geometric characteristics of these sulphide anomalies but also to rationalise the control drilling for a better evaluation of the reserves. This model of polymetallic sulphide deposit associated with shear zones provides insights into gold exploration throughout volcano-sedimentary trenches from subsaharian Africa and elsewhere.

Funding

No funding was provided for this study.

Acknowledgements

The authors are grateful to the *Société Nouvelle de Géophysique* for agreeing to make the field study data available to us as part of this university project.

Conflicts of Interest

The authors declare no conflicts of interest regarding the publication of this paper.

References

- Aka, E. B. J. C. (2018). *Geophysical Study by Magnetometry and Induced Polarization of the Precambrian Formations of Goumère Region (North-Eastern Côte d'Ivoire): Lithostructural Characterization and Implication to the Knowledge of Gold Mineralization* (191 p). Doctoral Thesis, Univ. Félix Houphouët-Boigny.
- Aka, E. B. J. C., Kouamé, E. L. N., Djroh, S. P., Oboue, Y. A. S. I., Gahe, E., & Sombo, B. C. (2017). Contribution of Geophysics to the Study of the Gold Mineralization of Goumère, North-East Côte d'Ivoire: Magnetometry and Induced Polarization. *Afrique Science*, 13, 261-272.
- Allou, G. (2014). *Study of the Volcano-Sedimentary Series of the Dabakala Region. Genesis and Magmatic Evolution: Contribution to the Knowledge of the Gold Mineralization of Bobosso in the Upper Comoe Series* (229 p). Doctoral Thesis, University of South Paris XI Sud-Paris.
- Coulibaly, I. (2018). *Petrography of the Volcanics and Plutonites of the Southern Part of the Toumodi-Fetekrotrench* (218 p). Thesis, Université Félix Houphouët-Boigny.
- Couture, R. (1968). *Geological Reconnaissance Map at 1/500,000 Scale, Sheet Odienne. Surveys Carried out from 1955 to 1961*. Dir. Mines et Geol.
- Djroh, S. P. (2014). *Geophysical Studies of the Samapleu Platinum-Bearing Cupronickel Deposit. 3D Modelling Test by Interpretation of Magnetic and Electrical Data* (176 p). Doctoral Thesis, Université Félix Houphouët-Boigny.
- Doumbia, I. (2013). *Lithostratigraphic and Metallogenic Study of the Sissédougou Gold Prospect on Boundiali Region* (50 p). DEA, University of Cocody.
- Fofana, K., Allialy, M. E., Coulibaly, I., & Teha, K. R. (2021). Geochemical Signature of the Granitoids of the Eastern Branch of the Boundiali-Korhogo Trench (Northern Côte d'Ivoire). *European Scientific Journal*, 17, 223-240.
- Gnanzou, A. (2014). *Study of the Volcano-Sedimentary Series of the Dabakala Region (North-East Côte d'Ivoire): Genesis and Magmatic Evolution. Contribution to the Knowledge of the Gold Mineralization of Bobosso in the Upper Comoe Series* (303 p). PhD Thesis, Université Paris-Saclay, and Université Félix Houphouët-Boigny.
- Heritiana, R., Riva, R., Ralay, R., & Boni, R. (2019). Evaluation of Flake Graphite Ore Using Self-Potential (SP), Electrical Resistivity Tomography (ERT) and Induced Polarization (IP) Methods in East Coast of Madagascar. *Journal of Applied Geophysics*, 169, 134-141. <https://doi.org/10.1016/j.jappgeo.2019.07.001>
- Houssou, N. (2013). *Petrological, Structural and Metallogenic Studies of the Gold Deposit of Agbahou, Divo* (177 p). PhD Thesis, Université Félix Houphouët-Boigny.
- Koffi, B. G., Ouattara, G., Kouamelan, A. N., & Derooin, J. P. (2013). Petro-Structurale Study of the Volcano-Plutonites of the Monts du Yaoure: Contribution to the Understanding of the Metalotectic Context of Gold Mineralization (Côte d'Ivoire). *International Journal of Innovation and Applied Studies*, 2, 635-644.
- Milesi, J. P., Feybesse, J. L., Ledru, P., Dommanget, A., Ouedraogo, M. F., Marcoux, E., Prost, A. E., Vinchon, C., Sylvain, J. P., Johan, V., Tegye, M., Calvez, J. Y., & Lagny P. (1989). The Gold Mineralization in West Africa. Their Relations with the Proterozoic Evolution Lithostructural. *Chronicle of Mining Research*, 497, 3-98.

- Miller, H. G., & Singh, V. (1994). Potential Field Tilt—A New Concept for Location of Potential Field Sources. *Journal of Applied Geophysics*, 32, 213-217.
[https://doi.org/10.1016/0926-9851\(94\)90022-1](https://doi.org/10.1016/0926-9851(94)90022-1)
- Moreira, C. A., Borssatto, K., Ilha, L. M., Dos, Santos S F., & Rosa, F. T. G. (2016). Geophysical Modelling in Gold Deposit through DC Resistivity and Induced Polarization Methods. *REM: International Engineering Journal*, 69, 293-299.
<https://doi.org/10.1590/0370-44672016690001>
- Ouattara, S. (2018). *The Dougbafla-Bandama Deposit (South of the Fétékrobiriman sillon, Oumé, Côte d'Ivoire): Petrography, Deformation, Geochemistry and Metallogeny* (252p). PhD Thesis, Université Félix Houphouët-Boigny.
- Ouattara, Z. (2015). *Lithostratigraphic, Structural, Geochemical and Metallogenic Characteristics of the Bonikro Gold Deposit, Fétékrobirimiansillon* (256 p). PhD Thesis, Université Félix Houphouët-Boigny.
- Sagax Geophysic Inc. (1989). *Induced Polarisation Surveys, Biencourt Project* (Internal Report, pp. 14-15). Sagax Geophysic Inc.
- Salem, A., Williams, S., Fairhead, J. D., Smith, R. & Ravat, D. J. (2008). Interpretation of Magnetic Data Using Tilt-Angle Derivatives. *Geophysics*, 73, 1-10.
<https://doi.org/10.1190/1.2799992>
- Sono, P., Nthaba, B., Shemang, E. M., Kgosidintsi, B., & Seane, T. (2020). An Integrated Use of Induced Polarization and Electrical Resistivity Imaging Methods to Delineate Zones of Potential Gold Mineralization in the Phitshane Molopo Area, Southeast Botswana. *Journal of African Earth Sciences*, 174, Article ID: 104060.
<https://doi.org/10.1016/j.jafrearsci.2020.104060>
- Tagini, B. (1971). *Structural Sketch of the Ivory Coast. Regional Geotectonics Essay* (University of Lausanne Bulletin No. 5, 302 p). Doctoral Thesis, SODEMI.
- Thurston, J. B., & Smith, R. S. (1997). Automatic Conversion of Magnetic Data to Depth, Dip and Susceptibility Contrast Using the SPITM Method. *Geophysics*, 62, 807-813.
<https://doi.org/10.1190/1.1444190>
- Verduzco, B. Fairhead, J. D., Green, C. M., & MacKenzie, C. (2004). New Insights into Magnetic Derivatives for Structural Mapping. *The Leading Edge*, 23, 116-119.
<https://doi.org/10.1190/1.1651454>
- Yacé, I. (2002). *Introduction to Geology. The Example of Côte d'Ivoire and West Africa* (183 p). Edition CEDA.